Eur. Phys. J. D **26**, 201–210 (2003)
DOI: 10.1140/epjd/e2003-00223-5

THE EUROPEAN PHYSICAL JOURNAL D

High resolution photo-absorption studies of acrylonitrile, C_2H_3CN, and acetonitrile, CH_3CN

S. Eden[1,a], P. Limão-Vieira[1,b], P. Kendall[1], N.J. Mason[1,c], S.V. Hoffmann[2], and S.M. Spyrou[3]

[1] Department of Physics and Astronomy, University College London, Gower Street, London WCIE 6BT, UK
[2] Institute for Storage Rings, University of Aarhus, Ny Munkegade, 8000 Aarhus C, Denmark
[3] Theoretical and Physical Chemistry Institute, National Hellenic Research Foundation, 48 Vas. Constantinou Ave., Athens 116 35, Greece

Received 7 January 2003 / Received in final form 5 May 2003
Published online 22 July 2003 –

Abstract. High resolution photo-absorption spectra of acrylonitrile and acetonitrile have been recorded in the wavelength range 115 to 320 nm (10.8 to 3.9 eV). Results are compared with previous photo-absorption measurements and electron energy loss spectra and, in most cases, are found to be in close agreement. The high resolution achieved in the present work has allowed some structures to be observed for the first time and new assignments have been suggested accordingly. The role of the molecules in the terrestrial atmosphere is discussed.

PACS. 32.30.Jc Visible and ultraviolet spectra

1 Introduction

Acrylonitrile, also known as vinyl cyanide and 2-propenitrile, does not occur naturally but is produced in great quantities industrially [1]. World production in 2000 was estimated at 4.6 million metric tons [2]. The compound is used primarily in the manufacture of acrylic fibres and as a raw material in the fabrication of plastics, nitrile rubbers and barrier resins. It also has applications in microelectronics as electrochemically thin films of the molecule can be deposited onto metallic substrates [3]. Acrylonitrile is released into the environment as gas and in waste water during its production and use. Other sources include auto-exhaust and release from fibres and plastics [4]. Due to the carbon-carbon double bond, acrylonitrile is expected to show enhanced reactivity towards atmospheric photo-oxidation by hydroxyl radicals and other oxidants.

Acetonitrile, otherwise known as methyl cyanide and ethanenitrile, is an important industrial gas. Though also used to make pesticides, its major application lies in the extraction of inorganic and organic chemicals, most importantly butadiene [5]. Acetonitrile also has the potential to be a tracer for biomass burning, considered the dominant source of the compound in the atmosphere [6]. In 1999, the global emission of acetonitrile from biomass burning was estimated to be between 0.4 and 1.0 Tgy^{-1} [7], compared to 0.02 Tgy^{-1} from fossil fuel burning reported in 2001 [8]. Chemically relatively inert, it has been observed in the stratosphere at concentrations of 110 to 160 parts per trillion by volume (pptv) [9].

The roles of acrylonitrile and acetonitrile in the atmosphere are not well understood. In particular, the residence times of the species in the stratosphere are subject to large errors. The mechanisms for airborne destruction of C_2H_3CN and CH_3CN therefore need to be re-examined. The VUV photo-absorption spectrum of acrylonitrile reported in this paper represents the highest resolution data yet published. Both results reveal new spectral detail and should allow better estimation the molecules' atmospheric lifetimes by photolysis.

2 Summary of the structure and properties of the molecules

The structure of acrylonitrile is derived from microwave spectroscopy [10,11]. The molecule is planar in the electronic ground state and belongs to the C_S symmetry group. Following the accepted sequence, the single C−H and C−C bonds are of σ character, while C=C comprises one σ and one π bond. The nitrogen atom is bound to a carbon atom (C−C≡N) by one σ and two π interactions. The two nitrogen electrons which

[a] e-mail: s.eden@ucl.ac.uk
[b] *Also at*: Departamento de Física, FCT - Universidade Nova de Lisboa, 2829-516 Caparica, Portugal and Centro de Física Molecular, Complexo I, IST, Av. Rovisco Pais, 1049-001 Lisboa, Portugal.
[c] *Also at*: Centre of Molecular and Optical Sciences, Department of Physics and Astronomy, The Open University, Walton Hall, Milton Keynes, MK7 6AA, UK.

do not take part in any bonds form a lone pair directed away from the molecule. The outermost valence molecular orbitals in the ground state of C_2H_3CN may be represented in the independent particle model as $(1a'')^2(11a')^2(12a')^2(2a'')^2$: $^1A'$ [12]. Acrylonitrile has 15 normal vibrational modes, eleven of which are symmetric (a') with respect to the molecular plane of symmetry and four anti-symmetric (a'') [13]. The vibrational modes considered to be excited in the present spectrum are υ_4 (a', C≡N stretching), υ_5 (a', C=C stretching), υ_8 (a', CH_2 rocking), υ_9 (a'', CHR=C wagging), υ_{10} (a'', CH_2=C wagging), and υ_{12} (a'', C=C torsion). In the neutral ground state, these excitations are given by Shimanouchi to occur at 0.278, 0.200, 0.136, 0.120, 0.118, and 0.085 eV, respectively [14].

The ground state geometrical configuration of acetonitrile is based on the analysis of rotational constants and X-ray diffraction spectra [15,16]. The molecule has C_{3v} symmetry. The methyl carbon is sp^3 hybridised, forming a σ bond with each of the hydrogen atoms and with the nitrogen bonding carbon atom, hybridised *sp* [17]. The nitrogen atom is similarly *sp* hybridised and forms one σ and two mutually perpendicular π bonds (C−C≡N). The two remaining nitrogen electrons form a lone pair directed away from the molecule. For the outermost valence molecular orbitals, the ground state of CH_3CN may be represented as $(4a_1)^2(5a_1)^2(6a_1)^2(1e)^4(7a_1)^2(2e)^4$: $^1A'$ [18]. Within the present analysis, features are assigned to five vibrational modes of excitation; υ_1 (C−H stretching), υ_2 (C≡N stretching), υ_3 (CH_3 deformation), υ_4 (C−C stretching), and υ_8 (C−C≡N bending) [14]. Of these modes, all but υ_8 are symmetric. Shimanouchi lists the neutral ground state excitation energies of the modes as 0.368, 0.281, 0.172, 0.114, and 0.045 eV, respectively.

3 Experimental

Photo-absorption spectra were taken at the ASTRID facility, Aarhus University, Denmark [19]. Briefly, synchrotron radiation is passed through a static gas sample. A photomultiplier is used to measure the transmitted light intensity at 0.05 nm intervals and wavelength is selected using a toroidal dispersion grating. Great care is taken to ensure there are no second-order light effects. The minimum and maximum wavelengths between which scans are performed, 115 to 320 nm (10.8 to 3.9 eV), are determined by the transmission windows of the gas cell and varied to give maximum absorption whilst avoiding saturation. The synchrotron beam ring current is monitored throughout the collection of each spectrum. Results are compared to a background scan recorded with the cell evacuated. Absolute photo-absorption cross-sections are generated using the Beer-Lambert law:

$$I_t = I_0 \exp(-n\sigma x) \quad (1)$$

where I_t is the radiation intensity transmitted through the gas sample, I_0 is that through the evacuated cell, n the molecular number density of the sample gas, σ the absolute photo-absorption cross-section, and x the absorption path length.

The apparatus is calibrated precisely before the capture of each spectrum. SO_2 is used to verify the energy scale as it shows bands with clearly defined sets of sharp absorption peaks in the ranges 3.8 to 5.1 eV [20] and 5.15 to 7.25 eV [21]. The Schuman-Runge (6.9–9.5 eV) absorption band of O_2 is used to calibrate the absolute cross-section because its broad nature minimises any errors due to different energy resolutions used in different experiments [22].

The experimental full width half maximum resolution for the present results may be taken to be 0.075 nm, corresponding to 1.5 meV over the energy range studied. This compares favourably with previous studies. Though not given explicitly, an indication of the resolution of the acrylonitrile spectrum of Mullen and Orloff [11] lies in the fact that wavelength was selected using a grating of 590 lines per mm [23] compared to 2000 lines per mm at the ASTRID facility [19]. For acetonitrile, the resolution of the spectrum of Suto and Lee is given as 0.08 nm, over the range 106 to 180 nm (11.7–6.9 eV) [24]. Nuth and Glicker [25] report the absolute absorption cross-section over the wavelength range 60 to 160 nm (20.7–7.7 eV) with a resolution of 0.05 nm. However, despite resolution being apparently no better, the present acetonitrile spectrum shows more detailed structure than previously reported. In particular, the peak at 10.501 eV is more clearly defined in the present work than in that of Nuth and Glicker. The spectrum of Suto and Lee shows no feature at 10.401 eV, visible both in the present work and in that of Nuth and Glicker.

The spectrum for acrylonitrile is compared to a previously unpublished photo-absorption result taken at the Daresbury Laboratory Synchrotron Radiation Source. The experimental set up is described in detail by Mason *et al.* [26]. The maximum resolution is estimated to be 0.1 nm.

Results are also compared to electron energy loss (EEL) spectra taken at the Université de Liège by Motte-Tollet *et al.* [12] and Gochel-Dupuis *et al.* [27] for acrylonitrile and acetonitrile, respectively. The overall energy resolution quoted in both works is around 30 meV.

C_2H_3CN and CH_3CN samples were purchased from Sigma Aldrich and have minimum purities of 99% and 99.5%, respectively. Gas was introduced to the cell following a series of freeze-pump-thaw cycles.

4 Results and discussion

4.1 Photo-absorption by acrylonitrile

Figure 1 shows the spectrum for incident photon energies between 5.5 and 10.8 eV, corresponding to the excitation of electrons belonging to the outer-most valence shell orbitals. No absorption is observed below 5.8 eV. The energy positions of the major features are in good agreement with the photo-absorption spectrum

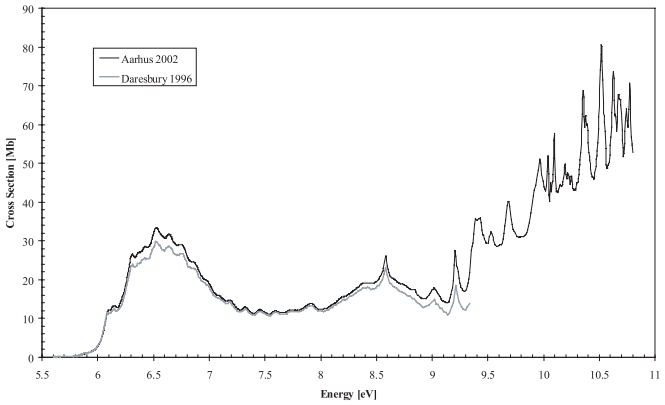

Fig. 1. High-resolution photo-absorption spectrum of C_2H_3CN recorded at the ASTRID Synchrotron ring facility compared with lower resolution result recorded at the Daresbury Laboratory Synchrotron Radiation Source.

reported by Mullen and Orloff [11] from 5.3 to 9.7 eV. The generalised shape and a number of the peaks observed are also consistent with the EELS results taken by Motte-Tollet *et al.* [12] using incident electrons of 50 eV and analysed at a scattering angle of 10° over an energy loss range of 5.5 to 11.5 eV. Under these conditions, electron scattering can be considered to simulate photon interactions [28]. The present photo-absorption spectrum shows a broad feature with maximum absorption at 6.526 eV attributed to promotion to the first excited electronic state, $\widetilde{A}^1A'$, corresponding to the $\pi_2(\text{C=C}-\text{C}\equiv\text{N}) \rightarrow \pi_1^*(\text{C=C}-\text{C}\equiv\text{N})$ transition [12]. The first peak for the second singlet excited electronic state $\widetilde{B}^1A''$, transition $\pi_2(\text{C=C}-\text{C}\equiv\text{N}) \rightarrow \pi^*(\text{C}\equiv\text{N})$, appears at 7.183 eV and the maximum for the third excited electronic state $\widetilde{C}^1A'$, $\pi_2(\text{C=C}-\text{C}\equiv\text{N}) \rightarrow \pi_2^*(\text{C=C}-\text{C}\equiv\text{N})$, at 8.580 eV. The broad structure observed is attributed to pre-dissociation combined with mutual overlap of the valence bands. The peaks above 8.6 eV are associated with Rydberg transitions. However, some mixing of valence and Rydberg transitions is observed, complicating the assignment of features.

4.1.1 Valence excitation of acrylonitrile in the energy range 5.5 to 8 eV

A detail of the spectrum in the energy region 5.5 to 8 eV is depicted in Figure 2. This region is dominated by an intense broad band extending with a local maximum of 33.31 Mb at 6.526 eV. Superimposed onto the extended structure are overlapping series of smaller peaks and shoulders. The energy values found for the associated vibrational structure are listed in Table 1 and compared with corresponding features observed by Mullen and Orloff [11] and Motte-Tollet *et al.* [12]. The energy precision to which some assignments can be given is limited by the diffuse nature of the features.

Table 1. Vibrational structure and assignments in the 5.5–7.1 eV absorption band of C_2H_3CN, for the lowest energy excited electronic state $\widetilde{A}^1A'$, corresponding to the $\pi_2(\text{C=C}-\text{C}\equiv\text{N}) \rightarrow \pi^*(\text{C=C}-\text{C}\equiv\text{N})$ transition (energies in eV).

Peak energy	Mullen and Orloff [11]	Motte-Tollet *et al.* [12]	Vibrational analysis
5.88^{D}	5.88	5.875	υ_{00}
6.102	6.11	6.10	$1\upsilon_4$
6.147	6.15	-	$1\upsilon_4 + 1\upsilon_{12}$
6.310	6.31	6.31	$2\upsilon_4$
6.38^{D}	6.38	-	$2\upsilon_4 + 1\upsilon_{12}$
6.427	6.43	-	$2\upsilon_4 + 2\upsilon_{12}$
6.526	6.53	6.525	$3\upsilon_4$
6.641	6.65	6.645	$3\upsilon_4 + 1\upsilon_9$ or $3\upsilon_4 + 1\upsilon_{10}$
6.738	6.74	6.75	$4\upsilon_4$
6.87^{D}	6.86	6.87	$4\upsilon_4 + 1\upsilon_9$ or $4\upsilon_4 + 1\upsilon_{10}$
6.97^{D}	6.97	7.00	$5\upsilon_4$
7.10^{D}	7.08	-	$5\upsilon_4 + 1\upsilon_9$ or $5\upsilon_4 + 1\upsilon_{10}$

Vibrational assignments are suggested for the first time in the present work. [D] Indicates that the feature is diffuse and thus its energy position is subject to greater uncertainy.

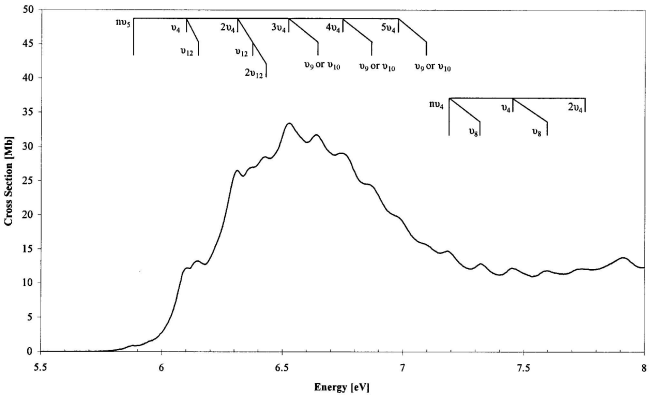

Fig. 2. Photo-absorption spectrum in the 5.5–8.0 eV band of C_2H_3CN.

Table 2. Vibrational structure and assignments in the 7.1–7.8 eV absorption band of C_2H_3CN, for the second excited electronic state $\widetilde{B}^1A''$, corresponding to the $\pi_2(\text{C=C}-\text{C}\equiv\text{N}) \rightarrow \pi^*(\text{C}\equiv\text{N})$ transition (energies in eV).

Peak energy	Mullen *et al.* [11]	Motte-Tollet *et al.* [12]	Vibrational analysis
7.183	7.19	7.185	υ_{00}
7.319	7.32	7.325	$1\upsilon_8$
7.451	7.46	7.455	$1\upsilon_4$
7.593	7.59	7.595	$1\upsilon_4 + 1\upsilon_8$
7.74^{D}	7.74	7.74	$2\upsilon_4$

[D] Indicates that the feature is diffuse and thus its energy position is subject to greater uncertainty.

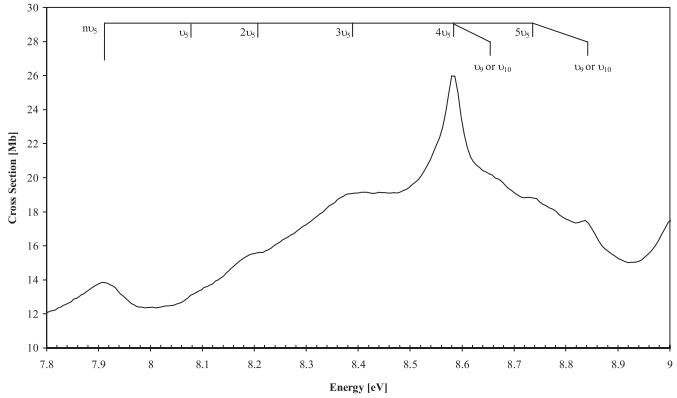

Fig. 3. Photo-absorption spectrum in the 7.0–9.0 eV band of C_2H_3CN.

Table 3. Vibrational structure and assignments in the 7.9–9.0 eV absorption band of C_2H_3CN, for the third excited electronic state $\widetilde{C}^1A'$, corresponding to the π_2(C=C−C≡N) → π_2^*(C=C−C≡N) transition (energies in eV).

Peak energy	Mullen *et al.* [11]	Motte-Tollet *et al.* [12]	Vibrational analysis
7.907	7.90	7.895	υ_{00}*
8.08^{D}	8.07	-	$1\upsilon_5$
8.21^{D}	8.24	-	$2\upsilon_5$
8.39^{D}	8.41	-	$3\upsilon_5$
8.580	-	8.595	$4\upsilon_5$*
8.65^{D}	8.67	-	$4\upsilon_5 + 1\upsilon_9$ or $4\upsilon_5 + 1\upsilon_{10}$
8.73^{D}	8.74	-	$5\upsilon_5$
8.837	-	8.84	$5\upsilon_5 + 1\upsilon_9$ or $5\upsilon_5 + 1\upsilon_{10}$

All the assignments given above are suggested for the first time in this work. ^{D} Indicates that the feature is diffuse and thus its energy position is subject to greater uncertainty. * Considered to overlap with Rydberg exitations.

The lowest energy feature is located at 5.88 eV and has been assigned in accordance with Motte-Tollet *et al.* [12] to the electronic excitation occurring from the highest occupied molecular orbital, π_2(C=C−C≡N), to the lowest singlet excited state, π_1^*(C=C−C≡N). The excited state is recognised as being of A' symmetry. Mullen and Orloff [11] observe a feature close to this energy but leave it unassigned, preferring to offer the peak at 6.11 eV as corresponding to the valence excitation and attributing the following structure to a υ_4 series, C≡N stretching. We propose a υ_4 series beginning at 5.88 eV with further features assigned to combinations of υ_4 with υ_{12} excitations and of υ_4 with either υ_9 or υ_{10}. The modes υ_9, υ_{10}, and υ_{12}, corresponding to CHR=C wagging, CH_2=C wagging, and C=C torsion, respectively, are anti-symmetric and thus would be expected to show very weak cross-section as single excitations [29]. However, double excitation or combination with another mode can increase the probability. As the neutral ground state excitation energies for υ_9 and υ_{10} are very similar, their symmetry equal and their motions similar, we do not suggest one or other as more probable. Note that we are reluctant to assign transitions to υ_{13}, υ_{14}, and υ_{15} as they are reported only by Raman spectroscopy for the liquid phase [13,14].

At the high end of the energy range of Figure 2, further vibrational structure is observed. The peaks are attributed to the transition from the outermost occupied orbital π_2(C=C−C≡N) → π^*(C≡N), assigned in accordance with Motte-Tollet *et al.* [12] as the second excited state $\widetilde{B}^1A''$. The vibrational analysis associated with this transition leads to a short series of $n\upsilon_4$ and $n\upsilon_4 + \upsilon_8$, CH_2 rocking, presented in Table 2.

The υ_{00} transition for this electronic band has been assigned at 7.183 eV.

4.1.2 Valence excitation of acrylonitrile in the energy range 7.8 to 9 eV

In this range, shown in detail in Figure 3, the spectrum consists of a fairly sharp peak with cross-section 25.96 Mb at 8.580 eV and a diffuse vibrational structure characterised by the modes υ_5 and υ_9 or υ_{10}. We suggest that the series of peaks is related to the population of the third valence excited state formed by the excitation of an electron from the outermost occupied orbital π_2(C=C−C≡N) → π_2^*(C=C−C≡N), of A' symmetry, in accordance with Motte-Tollet *et al.* [12]. The assignments for the third excited electronic state, $\widetilde{C}^1A'$, are given in Table 3. Previously, the associated structure could not be analysed fully due to nitrogen contamination. However, the peaks observed at 7.907 and 8.580 eV are assigned by Motte-Tollet *et al.* [12] to the Rydberg transitions $3s\sigma$ and $3p\lambda$. It is suggested here that these asymmetrical peaks represent superpositions of valence and Rydberg interactions.

4.1.3 Acrylonitrile Rydberg series

The higher energy range of the absorption spectrum is shown in detail in Figure 4. The peaks are attributed to Rydberg series converging to the ionisation potentials; 10.924, 12.353 and 13.107 eV [18]. To assign Rydberg states to series, the standard equation is used;

$$E_n = E_I - (R/(n-\delta)^2) \quad (2)$$

where E_n is the energy of the Rydberg state, E_I the ionisation limit to which the series converges (this may be the ionic ground state or an ionic excited state), R the Rydberg constant (13.61 eV), n the principal quantum number, and δ the relevant quantum defect.

The peak energies and Rydberg assignments converging to 10.924 eV, the ionic ground state $\widetilde{X}^2A''$, are shown in Table 4. Also shown in the table are the relevant quantum defects and suggested combinations of Rydberg and vibrational excitations to account for previously unassigned features. In agreement with previous work [12], the lowest energy peak attributed to a Rydberg transition, at 7.907 eV, is assigned as $3s\sigma$ in a series converging to 10.924 eV, the associated quantum defect being 0.88.

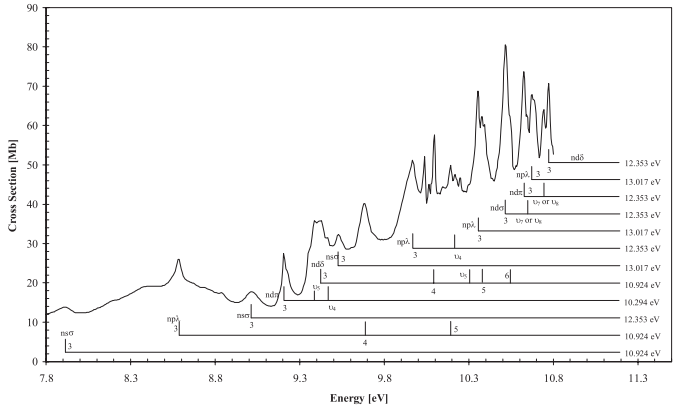

Fig. 4. Assignment of the C_2H_3CN Rydberg series occurring above 7.8 eV.

Table 4. Energy values, quantum defect and assignment of the Rydberg series converging to the ionic electronic ground state $\widetilde{X}^2A''$ of C_2H_3CN (energies in eV).

Peak energy	Motte-Tollet *et al.* [12]	Quantum defect	Assignment
7.907	7.895	0.88	$3s\sigma^*$
8.580	8.595	0.59	$3p\lambda^*$
9.679	9.703	0.69	$4p\lambda$
10.192	10.203	0.69	$5p\lambda$
9.205	9.215	0.19	$3d\pi$
9.386	-	-	$3d\pi + 1\upsilon_5^\bullet$
9.465	-	-	$3d\pi + 1\upsilon_4^\bullet$
9.429	9.415	0.02	$3d\delta$
10.097	10.103	0.06	$4d\delta$
10.30^D	10.26	-	$4d\delta + 1\upsilon_5$
10.380	-	0	$5d\delta^\bullet$
10.54^D	-	0.03	$6d\delta^\bullet$

$^\bullet$ Accompanies assignments suggested for the first time in the present work. ^{D} Indicates that the feature is diffuse and thus its energy position is subject to greater uncertainty. * Considered to overlap with valence excitations (Tab. 3).

The peak at 8.580 eV is assigned to an $np\lambda$ progression including $n = 3$, 4, and 5, converging to the first ionisation limit. The peak at 9.205 eV is considered to match that observed by Motte-Tollet *et al.* [12] at 9.215 eV, assigned to the $n = 3$ term of an $nd\pi$ series with δ equal to 0.19. Recognition of this feature leads us to suggest two further assignments corresponding to the combination of vibrational excitation and the Rydberg transition $3d\pi$. The photoelectron work of Delwiche *et al.* [18] reports vibrational progressions of υ_4 and υ_5 for the 10.924 eV band with energies 0.248 and 0.180 eV, respectively, matching closely the energy differences observed between the $3d\pi$ transition and the assigned vibrational structure in the present spectrum. The assignments to $3d\delta$ and $4d\delta$ transitions and to $4d\delta + \upsilon_5$ excitation are made in agreement with Motte-Tollet *et al.* [12]. The peak at 10.380 eV and the shoulder at 10.54 eV are tentatively added to the $nd\delta$ series, converging to 10.924 eV.

Table 5. Energy values, quantum defect and assignment of the Rydberg series converging to 12.353 eV, the ionisation limit corresponding to ionic electronic first excited state $\widetilde{A}^2A'$ of C_2H_3CN (energies in eV).

Peak energy	Motte-Tollet *et al.* [12]	Quantum defect	Assignment
9.017	9.055	0.98	$3s\sigma$
9.967	9.963	0.61	$3p\lambda$
10.217	-	-	$3p\lambda + 1\upsilon_4$
10.516	10.527	0.28	$3d\sigma$
10.64^D	-	-	$3d\sigma + 1\upsilon_7$ or $3d\sigma + 1\upsilon_8$
10.624	10.643	0.20	$3d\pi$
10.744	-	-	$3d\pi + 1\upsilon_7$ or $3d\pi + 1\upsilon_8$
10.772	10.783	0.07	$3d\delta$

Vibrational assignments are suggested for the first time in the present work. ^{D} Indicates that the feature is diffuse and thus its energy position is subject to greater uncertainty.

Table 6. Energy values, quantum defect and assignment of the Rydberg series converging to 13.017 eV, the ionisation limit corresponding to the ionic electronic second excited state $\widetilde{B}^2A'$ of C_2H_3CN (energies in eV).

Peak energy	Motte-Tollet *et al.* [12]	Quantum defect	Assignment
9.530	9.547	1.03	$3s\sigma$
10.354	10.379	0.74	$3p\lambda$
10.675	10.695	0.59	$3p\lambda$

The peaks considered to be related to Rydberg series converging on the ionic electronic first excited state, $\widetilde{A}^2A'$ are listed in Table 5. The ionisation potential associated with this state is 12.353 eV and the series are located above 9 eV. Within our spectral range only the lowest energy, $n = 3$ terms amongst the previously assigned $ns\sigma$, $np\lambda$, $nd\sigma$, $nd\pi$ and $nd\delta$ series [12] are observed. Delwiche *et al.* [18] report a υ_4 series with excitation energy 0.248 eV for this state and a further vibrational series with energy difference 0.148 eV, suggested to be consistent either with the υ_7 or υ_8 vibrational modes, CH rocking and CH_2 rocking, respectively. The present vibrational assignments are made accordingly.

Three series in the energy range of this spectrum are suggested to converge on the ionisation potential 13.017 eV, associated with the ionic electronic second excited state, $\widetilde{B}^2A'$. The recommended assignments are given in Table 6. Peaks at 9.530, 10.354 and 10.675 eV are assigned in accordance with Motte-Tollet *et al.* [12] to transitions $3s\sigma$, $3p\lambda$ and $3p\lambda$. Shoulders at 9.22 and 9.73 eV and peaks at 10.039, 10.684, 10.064 and 10.247 eV are observed but remain unassigned.

4.2 Photo-absorption by acetonitrile

Figure 5 shows the spectrum from incident photon energy 7 to 10.8 eV and includes details of the energy

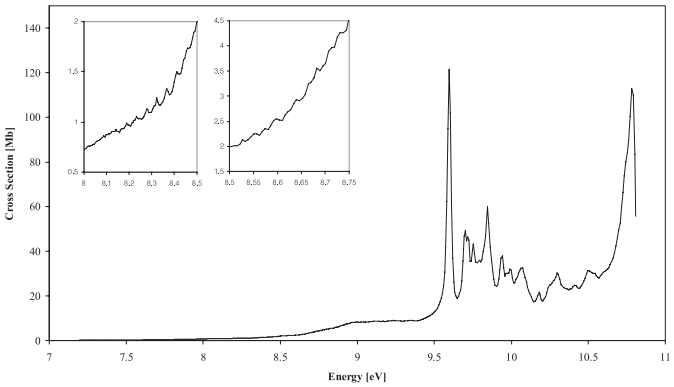

Fig. 5. High-resolution photo-absorption spectrum of CH_3CN recorded at the ASTRID Synchrotron ring facility.

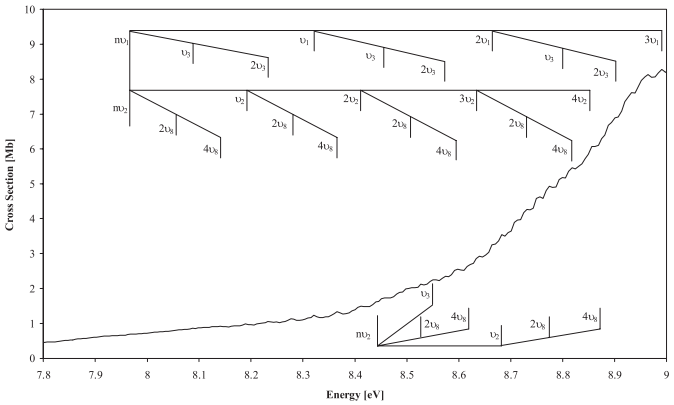

Fig. 6. Photo-absorption spectrum in the 7.8–9.0 eV band of CH_3CN.

region 8.00 to 8.75 eV to demonstrate the presence of vibrational structure. The shape of the spectrum and energy positions of the major features are in good agreement with the photo-absorption spectrum taken by Suto and Lee [24], Nuth and Glicker [25], and with the EELS results of Gochel-Dupuis *et al.* [27]. From around 6.8 eV there rises a broad feature with a maximum cross-section of 9.180 Mb occurring at 9.350 eV before a series of strongly absorbing sharp peaks dominate the spectrum over the remaining range. The sharp peaks are assigned to Rydberg transitions [24,25,27,30]. However, as with acrylonitrile, analysis is complicated by some mixing of valence and Rydberg series. The low energy feature is associated with the valence transitions $2e \rightarrow 3e(\pi \rightarrow \pi^*)$ and $7a_1 \rightarrow 3e(n_N \rightarrow \pi^*)$ superimposed on a background caused by pre-dissociation [27]. Although no absorption is observed in the present work below 7 eV, it should be noted that Gochel-Dupuis *et al.* [27] report features at low energies, associated with optically forbidden states.

4.2.1 Valence excitation of acetonitrile in the range 7.8 to 9 eV

The absorption cross-section in this energy range is shown in detail in Figure 6. The structure is considered to be caused by the transition $2e \rightarrow 3e(\pi \rightarrow \pi^*)$. Analysis of the peaks suggests the presence of υ_1, υ_2 and υ_3 series beginning around 7.95 eV, the energy loss at which Gochel-Dupuis *et al.* [27] observe a small peak using incident electrons of 25 eV and a scattering angle of 30°, attributable to an optically forbidden excitation [29]. Therefore, the transition is tentatively assigned at 7.97 eV, the energy that appears to match best the pattern of vibrational structure observed in the present work.

Table 7 lists the energies of the features observed between 7.9 and 9 eV. Gochel-Dupuis *et al.* [27] propose the presence of υ_2 progressions starting at 7.95 and 8.44 eV. Structure observed for the first time in this work leads us to suggest further sets of assignments. From 7.97 eV there appears to be two overlapping series of vibrational excitations. The first is associated with υ_1, corresponding

Table 7. Vibrational structure and assignments in the 7.9–9 eV absorption band of CH_3CN, corresponding to the $2e \rightarrow 3e(\pi \rightarrow \pi*)$ transition (energies in eV).

Peak energy	Gochel-Dupuis *et al.* [27]	Vibrational analysis
7.97*	7.95	υ_{00}
8.09^{D}	-	υ_3
8.23^{D}	-	$2\upsilon_3$
8.321	-	υ_1
8.46^{D}	-	$\upsilon_1 + \upsilon_3$
8.574	-	$\upsilon_1 + 2\upsilon_3$
8.66^{D}	-	$2\upsilon_1$
8.800	-	$2\upsilon_1 + \upsilon_3$
8.92^{D}	-	$2\upsilon_1 + 2\upsilon_3$
8.991	-	$3\upsilon_1$
8.06^{D}	-	$2\upsilon_8$
8.14^{D}	-	$4\upsilon_8$
8.19^{D}	-	υ_2
8.277	-	$\upsilon_2 + 2\upsilon_8$
8.366	-	$\upsilon_2 + 4\upsilon_8$
8.411	-	$2\upsilon_2$
8.51^{D}	-	$2\upsilon_2 + 2\upsilon_8$
8.598	-	$2\upsilon_2 + 4\upsilon_8$
8.64^{D}	-	$3\upsilon_2$
8.731	-	$3\upsilon_2 + 2\upsilon_8$
8.818	-	$3\upsilon_2 + 4\upsilon_8$
8.856	-	$4\upsilon_2$
8.44^{D}	8.44	υ_{00}
8.527	-	$2\upsilon_8$
8.62^{D}	-	$4\upsilon_8$
8.682	-	υ_2
8.775	-	$\upsilon_2 + 2\upsilon_8$
8.88^{D}	-	$\upsilon_2 + 4\upsilon_8$

All the assignments for vibrational excitations listed above are suggested for the first time in the present work. ^{D} Indicates that the feature is diffuse and thus its energy position is subject to greater uncertainty. * This energy was chosen purely on the basis of the following vibrational structure as described in the text.

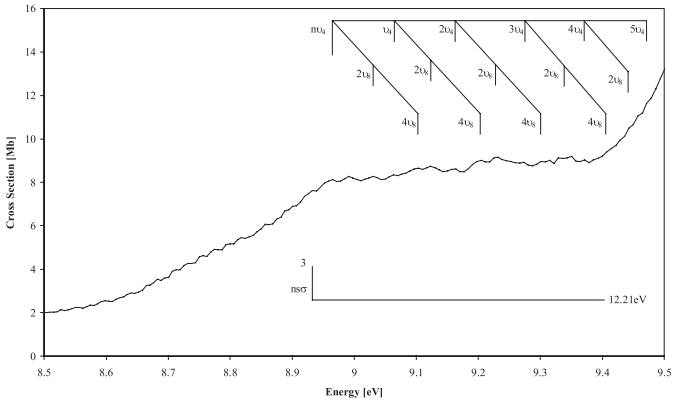

Fig. 7. Photo-absorption spectrum in the 8.5–9.5 eV band of CH_3CN.

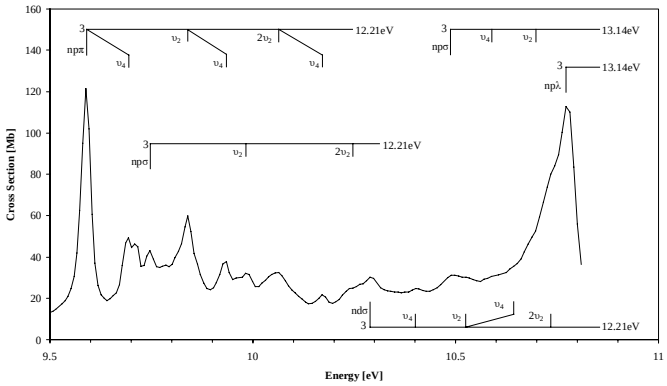

Fig. 8. Assignment of the CH_3CN Rydberg series occurring above 9.5 eV.

Table 8. Vibrational structure and assignments in the 8.9–9.5 eV absorption band of CH_3CN, corresponding to the $7a_1 \rightarrow 3e(n_N \rightarrow \pi*)$ transition (energies in eV).

Peak energy	Gochel-Dupuis *et al.* [27]	Vibrational analysis
8.965	8.96	υ_{00}
9.030	-	$\upsilon_{00} + 2\upsilon_8$
9.103	-	$\upsilon_{00} + 4\upsilon_8$
9.063	9.07	υ_4
9.123	-	$\upsilon_4 + 2\upsilon_8$
9.205	-	$\upsilon_4 + 4\upsilon_8$
9.164	9.18	$2\upsilon_4$
9.232	-	$2\upsilon_4 + 2\upsilon_8$
9.301	-	$2\upsilon_4 + 4\upsilon_8$
9.273	9.29	$3\upsilon_4$
9.34^{D}	-	$3\upsilon_4 + 2\upsilon_8$
9.41^{D}	-	$3\upsilon_4 + 4\upsilon_8$
9.372	-	$4\upsilon_4$
9.44^{D}	-	$4\upsilon_4 + 2\upsilon_8$
9.47^{D}	-	$5\upsilon_4$

All the assignments for vibrational excitations listed above are suggested for the first time in the present work. ^{D} Indicates that the feature is diffuse and thus its energy position is subject to greater uncertainty.

to C−H stretching, with a limited υ_3 series beginning at each υ_1 peak. The mode υ_3 is symmetric and characterised by CH_3 deformation. The second series is attributed to vibrational excitation consistent with C≡N bending, the υ_2 mode. We propose that double excitations of the anti-symmetric υ_8 mode, corresponding to C−C≡N bending, combine with the υ_2 progression to give further small peaks. In agreement with Gochel-Dupuis *et al.* [27], a υ_2 excitation beginning at 8.44 eV is identified. The diffuse feature observed at 8.93 eV and attributed to a Rydberg transition may include a $2\upsilon_2$ contribution from this series. As with the previous series, combinations of double υ_8 excitations are suggested to account for further peaks and shoulders. Features observed at 8.49, 8.71 and 8.756 eV remain unassigned.

4.2.2 Valence excitation of acetonitrile in the range 8.9 to 9.5 eV

The valence transition $7a_1 \rightarrow 3e(n_N \rightarrow \pi^*)$ to the singlet state ^1E is considered to be responsible for the series of peaks beginning at 8.965 eV. The absorption spectrum for this energy range is shown in Figure 7. Gochel-Dupuis *et al.* [27] report three quanta of vibration with 0.110 eV mean spacing which they attribute to excitation of the υ_7 mode, CH_3 rocking. However, according to structure observed for the first time in the present work, we propose a υ_4 series, corresponding to C−C stretching, combined with double excitations of the mode υ_8. The observed peaks and their suggested assignments are listed in Table 8.

4.2.3 Acetonitrile Rydberg series

Figure 8 shows the absorption observed between 9.5 and 10.9 eV; the part of energy range scanned in the present work within which Rydberg transitions are known to occur. The suggested series converge to 12.21 and 13.14 eV, corresponding to the ionic electronic ground state and the ionic first excited state of CH_3CN, respectively [31].

The peak energies assigned to series converging to 12.21 eV are given in Table 9. The low energy, low intensity peak at 8.93 eV (shown in Fig. 7) is assigned to the Rydberg transition $3s\sigma$ as suggested by Nuth and Glicker [25]. The three peaks at 9.589, 9.747 and 10.289 eV are attributed to the $n = 3$ transition of the $np\pi$, $np\sigma$ and $nd\sigma$ series converging to the ionic electronic ground state [25,27]. In agreement with Gochel-Dupuis *et al.* [27], we suggest vibrational progressions beginning at Rydberg peaks as responsible for further structure. The vibrational modes suggested are υ_2 and υ_4, related to C≡N stretching, and C−C stretching, respectively. This is consistent with the photoelectron work of Turner *et al.* [31] which shows the energy required for the excitation of υ_2 and υ_4 in the first ionic state to be 0.249 eV and 0.100 eV, very close to the energy differences observed.

Table 10 gives the energies of the peaks assigned to Rydberg series converging to the second ionisation potential, 13.14 eV. In accordance with Gochel-Dupuis *et al.* [27]

Table 9. Energy values, quantum defect and assignment of the Rydberg series converging to 12.21 eV, the ionisation limit corresponding to the ionic electronic ground state of CH_3CN, (energies in eV).

Peak energy	Nuth and Glicker [25]	Gochel-Dupuis *et al.* [27]	Quantum defect	Assignment
8.93^{D}	8.930	-	0.96	$3s\sigma$
9.589	9.595	9.589	0.72	$3p\pi$
9.694	9.695	9.694	-	$3p\pi + \upsilon_4$
9.840	9.842	9.838	-	$3p\pi + \upsilon_2$
9.935	9.935	9.929	-	$3p\pi + \upsilon_2 + \upsilon_4$
10.064	10.056	10.060	-	$3p\pi + 2\upsilon_2$
10.171	10.181	10.182	-	$3p\pi + 2\upsilon_2 + \upsilon_4$
9.747	9.678	9.745	0.65	$3p\sigma$
9.983	9.983	9.973	-	$3p\sigma + \upsilon_2$
10.25^{D}	-	-	-	$3p\sigma + 2\upsilon_2^{\bullet}$
10.289	10.292	10.286	0.34	$3d\sigma$
10.401	-	10.415	-	$3d\sigma + \upsilon_4$
10.53^{D}	10.501	10.531	-	$3d\sigma + \upsilon_2$
10.64^{D}	-	-	-	$3d\sigma + \upsilon_2 + \upsilon_4^{\bullet}$
10.74^{D}	10.744	-	-	$3d\sigma + 2\upsilon_2^{\bullet}$

$^{\bullet}$ Accompanies assignments suggested for the first time in the present work. These assignments are subject to greater uncertainty.
^{D} Indicates that the feature is diffuse and thus its energy position is subject to greater uncertainty.

Table 10. Energy values, quantum defect and assignment of the Rydberg series converging to 13.14 eV, the ionisation limit corresponding to the ionic electronic first excited state of CH_3CN, (energies in eV).

Peak energy	Nuth and Glicker [25]	Gochel-Dupuis *et al.* [27]	Quantum defect	Assignment
10.489	10.501	10.520	0.74	$3p\sigma$
10.59^{D}	-	-	-	$3p\sigma + \upsilon_4$
10.70^{D}	-	-	-	$3p\sigma + \upsilon_2$
10.772	10.777	10.780	0.60	$3p\lambda$

Vibrational assignments are suggested for the first time in the present work. These assignments are subject to greater uncertainty.
^{D} Indicates that the feature is diffuse and thus its energy position is subject to greater uncertainty.

the peaks at 10.489 and 10.772 eV are both attributed to the $n = 3$ transitions in the $3p\sigma$ and $np\lambda$ serie, respectively. Previously unassigned features at 10.59 eV and 10.70 eV are attributed to vibrational excitations along the modes υ_4 and υ_2 combined with the Rydberg transition at 10.489 eV, noted as having symmetry a_1. The features observed at 9.709 and 9.786 eV remain unassigned.

4.3 Absolute absorption cross-sections and atmospheric photolysis rates for acrylonitrile and acetonitrile

The cross-sectional values of acrylonitrile corresponding to energies between 6 and 9.5 eV are compared to the data of Mullen and Orloff [11] at steps of 0.5 eV. The peak values at 6.526 and 8.580 eV are also compared. The present measured cross-section is around 400% higher than that of Mullen and Orloff. To our knowledge, no other acrylonitrile photo-absorption data has been published over the range of the present spectrum. We are confident that our measured absolute cross-section is reliable due to the thorough calibration procedure described in Section 3. In addition, as shown in Figure 1, the present result is in good agreement with the lower resolution result recorded at the Synchrotron Radiation Facility, Daresbury, UK. The cross-sections measured at the two facilities match to within 10%, with the exception of a difference of 35% observed at 9.429 eV for the sharp Rydberg peak positioned in the high energy extreme of the spectral range available at Daresbury. Erroneous low cross-section values may result from a fall in optical transmission close to the experimental cut off frequency. The estimated error in absolute photo-absorption cross-section for a previous result taken using the Daresbury apparatus is given as $\pm$ 20% [32].

The atmospheric photolysis lifetime of acrylonitrile has been modelled using a program developed at University College London. The program considers a simplified system and evaluates the photolysis rate as a product of the solar actinic flux and the molecular photo-absorption cross-section at different wavelengths and altitudes [33]. The residence time is calculated for a molecule at a fixed altitude in a sunlit, clear atmosphere. The rate of photolysis of acrylonitrile is found this way to be of the order 10^{-4} s^{-1} in the stratosphere and 10^{-6} s^{-1} at lower altitudes. These rates give stratospheric residence times by photolysis in the order of hours. In the troposphere,

the calculated residence time rises from around 10 days at higher altitudes to over one year below 15 km. Thus, at altitudes below around 20 km, our result is consistent with previous understanding that degradation occurs dominantly by reactions with photochemically produced hydroxyl radicals [4]. The half life of acrylonitrile by these processes is estimated to be between 1 and 3.5 sunlit days, depending on conditions.

Comparison is made between the photo-absorption cross-section of acetonitrile reported in the present paper with that of Suto and Lee [24]. The two sets of data are found to be in agreement to within the limits of the error in reading the absorption plot of Suto and Lee. However, analysis of the three highest peaks, at 9.589, 9.840 and 10.772 eV, shows the present data to be 10 to 20% higher. This may be due to higher energy resolution for our spectrum. The major peaks appear sharper in the present work and, importantly, absorption at 9.589 eV is greater than at 10.772 eV whereas Suto and Lee observe the opposite. The only other photo-absorption data for acetonitrile published for photon energies coinciding with our range is the work of Nuth and Glicker [25]. Suto and Lee consider their result to agree with that of Nuth and Glicker to within the experimental uncertainties [24]. However, in agreement with our data, Nuth and Glicker clearly show the cross-section at 9.589 eV to be greater than at 10.772 eV. Thus, it can be concluded that the present spectrum is broadly consistent with previous photo-absorption results although it reveals stronger absorption for narrow features, suggesting higher energy resolution.

Suto and Lee estimate the photolysis rate of acetonitrile to be *very slow* in the troposphere and less than 10^{-11} s^{-1} in the stratosphere [24]. Thus, low altitude destruction of acrylonitrile is dominated by reactions with atmospheric species. In particular, the stratospheric reaction rate of CH_3CN + OH is estimated to be 10^{-7} s^{-1} using the data of Kurylo and Knable [34] and Heicklen [35]. No meaningful result could be achieved using our model as the absorption of acetonitrile is extremely weak below 7 eV. Minimal solar radiation above 7 eV is observed in the stratosphere and troposphere [36]. The Lyman α peak for solar radiation, considered the key region for photolysis of acetonitrile in the upper atmosphere, is very close to the absorption peak at 9.840 eV, observed to be around 20% stronger in the present spectrum than in that of Suto and Lee. Thus we would predict a slightly higher photolysis rate at high altitudes than that estimated previously whilst expecting that the overall atmospheric destruction of acetonitrile occurs dominantly through chemical reactions.

4.4 Comparison of acrylonitrile with acetonitrile

The photo-absorption spectra for C_2H_3CN and CH_3CN in the valence bands are dominated by transitions from π to π^* C≡N orbitals. For both molecules, these transitions feature C≡N bonds. In the case of acrylonitrile, the valence excitations observed are assigned to π_2(C=C−C≡N) $\rightarrow$ π_1^*(C=C−C≡N), π_2(C=C−C≡N) $\rightarrow$ π^*(C≡N), and π_2(C=C−C≡N) $\rightarrow$ π_2^*(C=C−C≡N). For acetonitrile, the lowest observed valence band is assigned to π(C−C≡N) $\rightarrow$ π^*(C−C≡N). For both molecules, C−H excitation is limited because of the very stiff nature of the bonds. This is evident in the observed vibrational excitations. For acrylonitrile, by far the most commonly assigned modes are υ_4 and υ_5, corresponding to C≡N and C=C stretching, respectively. Similarly, the dominant symmetric modes for vibrational excitation of acetonitrile are considered to be C≡N and C−C stretching, υ_2 and υ_4. The C−C≡N bending mode for acetonitrile, υ_8, also seems to be very readily excited.

A significant difference, however, is observed when we compare nitrogen lone pair excitations for each molecule. Excitation from the nitrogen lone pair electrons of acrylonitrile is not visible in the present range. However, the transition $n_N \rightarrow \pi^*$(C−C≡N) makes a significant contribution to the spectrum of acetonitrile. The lone pair for acrylonitrile lies in an orbital separated from the lowest unoccupied orbital by the $(12a')^2$ and $(2a'')^2$ orbitals, whereas that for acetonitrile is only separated by the occupied $(2e)^4$ orbital. Therefore, we would expect excitation from the lone orbital of CH_3CN to require markedly lower energy than that of C_2H_3CN and thus appear in the photo-absorption spectrum.

Comparison of Figures 1 and 5 shows that photo-absorption by acrylonitrile is greater at low energies than by acetonitrile. Thus, in the lower atmosphere, the photolysis rate of acrylonitrile is significant whereas we would not expect it to make a noticeable contribution to the destruction of acetonitrile. Both molecules absorb strongly at short wavelengths. However, no significant similarity in the Rydberg structures of acrylonitrile and acetonitrile is apparent within the energy range of this work.

5 Conclusion

Photo-absorption spectra of acrylonitrile and acetonitrile have been recorded in the wavelength range 115 to 320 nm (10.8 to 3.9 eV). High resolution has allowed several features to be observed for the first time and new assignments have been suggested accordingly. Results are compared to previous photo-absorption measurements and electron energy loss spectra and are found to be in close agreement in terms of the energy positions at which features are observed. More significant variation is evident when comparing the absolute cross-sections of bands. In the case of acrylonitrile, significantly higher absorption is observed in the present work than previously reported. This suggests the molecule has a shorter residence time in the stratosphere than expected. It would be instructive to incorporate the present results into a detailed atmospheric model to reevaluate quantitatively the residence times and the environmental effects of acrylonitrile and acetonitrile.

SE, PK and NJM acknowledge the support of the UK funding councils EPSRC, NERC and CLRC during the course of this research. PLV acknowledges financial support from the

Portuguese Foundation for Science and Technology. We also acknowledge the EU for funding the visit to the Aarhus synchrotron facility and Prof. M.-J. Hubin-Franskin and Prof. J. Delwiche of the Université de Liège, Belgium, for their valuable advice. Dr. N.C. Jones of the University of Aarhus, Denmark is acknowledged for providing the photo-absorption data measured at the Daresbury Laboratory Synchrotron Radiation Source.

References

1. www.epa.gov/opptintr/chemfact/acry-fs.txt
2. http://ceh.sric.sri.com/Public/Reports/607.5000/
3. G. Lécayon, Y. Barizem, C. Le Gressua, C. Juret, C. Reynaud, C. Boiziau, Chem. Phys. Lett. **91**, 506 (1982)
4. www.speclab.com/compound/C107131.html
5. www.epa.gov/opptintr/chemfact/f_acenit.txt
6. J.M. Lobert, D.H. Scharffe, W.M. Hao, P.J. Crutzen, Nature **346**, 552 (1990)
7. R. Holzinger, C. Warneke, A. Hansel, A. Jordan, W. Lindinger, D.H. Scharffe, G. Schade, P.J. Crutzen, Geophys. Res. Lett. **26**(8), 1161 (1999)
8. R. Holzinger, A. Jordan, A. Hansel, W. Lindinger, J. Atmosph. Chem. **38**(2), 187 (2001)
9. J. Schneider, V. Burger, F. Arnold, J. Geophy. Res. – Atmosph. **102**(D21), 25501 (1997)
10. C.C. Costain, B.P. Stoicheff, J. Chem. Phys. **43**, S129 (1965)
11. P.A. Mullen, M.K. Orloff, Theoret. Chim. Acta (Berl.) **23**, 278 (1971)
12. F. Motte-Tollet, D. Messina, M.-J. Hubin-Franskin, J. Chem. Phys. **103**(1), 80 (1995)
13. F. Halverson, R.F Stamm, J.J. Whalen, J. Chem. Phys. **16**, 080 (1948)
14. T. Shimanouchi, *Tables of Molecular Vibrational Frequencies Consolidated* (National Bureau of Standards, 1972), Vol. 1, pp. 1-160
15. G.L. Gutsev, A.L. Sobolewski, L. Adamowicz, Chem. Phys. **196**, 1 (1995)
16. K. Kwak, S. Cha, M. Cho, J.C. Wright, J. Chem. Phys. **117**(12), 5675 (2002)
17. www.staff.ncl.ac.uk/j.g.smith/chy002/chy002.html
18. J. Delwiche, M. Gochel-Dupuis, J.E. Collin, J. Heinesch, J. Electron Spectrosc. Rel. Phenom. **66**, 65 (1993)
19. www.isa.au.dk/SR/UV1/uv1.html
20. A.C. Vandaele, P.C. Simon, J.M. Guilmot, M. Carleer, R. Colin, J. Geophy. Res. – Atmosph. **99**(D12), 25599 (1994)
21. D.E. Freeman, K. Yoshino, J.R. Esmond, W.H. Parkinson, Planet. Space Sci. **32**, 1125 (1984)
22. K. Watanabe, Adv. Geophys. **5**, 153 (1958)
23. P.A. Mullen, M.K. Orloff, J. Mol. Spectrosc. **30**, 140 (1969)
24. M. Suto, L.C. Lee, J. Geophys. Res. **90**(D7), 13037 (1985)
25. J.A. Nuth, S. Glicker, J. Quant. Spectrosc. Radiat. Transfer **28**, 223 (1982)
26. N.J. Mason, J.M. Gingell, J.A. Davies, H. Zhao, I.C. Walker, M.R.F. Siggel, J. Phys. B **29**, 3075 (1996)
27. M. Gochel-Dupuis, J. Delwiche, M.-J. Hubin-Franskin, J.E. Collin, F. Edard, M. Tronc, J. Am. Chem. Soc. **112**, 5425 (1990)
28. R.H. Huebner, R.J. Celotta, S.R. Mielczarak, C.E. Kuyatt, J. Chem. Phys. **59**, 5434 (1973)
29. G. Herzberg, *Molecular Spectra and Molecular Structure III. Electronic Spectra and Electronic Spectra of Polyatomic Molecules* (Van Nostrand, New York, 1966)
30. C. Fridh, J. Chem. Soc., Faraday Trans. 2 **74**, 2193 (1978)
31. D.W. Turner, C. Baker, A.D. Baker, C.R. Brundle, *Molecular Photoelectron Spectroscopy* (Wiley, New York, 1970)
32. F. Motte-Tollet, M.-P. Ska, G.M. Marston, I.C. Walker, M.R.F. Siggel, J.M. Gingell, L. Kaminski, K. Brown, N.J. Mason, Chem. Phys. Lett. **275**, 298 (1997)
33. P. Limão Vieira, S. Eden, P.A. Kendall, N.J. Mason, S.V. Hoffmann, Chem. Phys. Lett. **364**, 535 (2002)
34. M.J. Kurylo, G.L. Knable, J. Phys. Chem. **88**, 3305 (1984)
35. J. Heicklen, *Atmosphere Chemistry* (Academic, Orlando, Fla., 1976)
36. Chemical Kinetics and Photochemical Data for Use in Stratospheric Modelling, Evaluation number 12, NASA, Jet Propulsion Laboratory, JPL Publication 97-4, January 15, 1997